SPE 133533

Transient Behavior and Analysis of Non-Darcy Flow in Porous and Fractured Reservoirs According to the Barree and Conway Model

Ajab Al-Otaibi and Yu-Shu Wu, Colorado School of Mines

This paper was prepared for presentation at the Western North America Regional Meeting held in Anaheim, California, USA, 26–30 May 2010.

Abstract

This study introduces the usage of the Barree and Conway flow model in well testing pressure-transient applications for a single-phase non-Darcy flow in porous and fractured reservoirs. The non-Darcy flow behavior is handled using a three-dimensional, general purpose reservoir simulator. This numerical model incorporates non-Darcy flow effect according to the Barree and Conway flow model and the developed numerical model is capable of simulating all near wellbore effects, such as the wellbore storage and skin effects, coupled with the non-Darcy flow behavior. In addition, a steady-state non-Darcy radial flow solution is derived analytically according to the Barree and Conway model. The numerical simulation results are verified with the analytical solution.

The numerical model is used to model and interpret the radial flow pressure-transient responses for both pressure buildup and drawdown well tests in porous and fractured reservoirs. In simulating pressure drawdown tests with the non-Darcy flow effects according to Barree and Conway model and assuming no skin and wellbore storage effects, the permeability, estimated using the standard straight-line analysis, is an apparent permeability and not the Darcy's constant permeability. The estimated permeability ranges from the minimum permeability and to less than the Darcy's permeability. Thus in pressure drawdown tests the standard straight-line analysis techniques underestimate the Darcy's permeability when non-Darcy flow behavior exists. A pressure buildup test, following non-Darcy flow drawdown tests, may be good for determining Darcy's permeability values using standard straight-line analysis when non-Darcy flow effect is insignificant. The Barree and Conway non-Darcy flow model parameters may not be directly estimated from the pressure-transient well tests with a simple graphic approach. However, they can be estimated by a matching process, based on non-linear optimization algorithm incorporated into the developed numerical model. The type curves generated by the numerical model are provided to demonstrate a methodology for modeling single phase transient non-Darcy flow behavior in porous and fractured rocks. The developed numerical model in this study is used to interpret and match actual pressure drawdown and buildup well tests from wells of high production rates in Kuwait.

Introduction

Darcy's law has been the fundamental principle in describing the fluid flow in porous media (Darcy, 1856). It describes a linear relationship between volumetric flow rate (Darcy velocity) and pressure (head or potential) gradient (Muskat, 1946). Darcy's law relates the pressure gradient to the fluid superficial velocity and through a constant k known as permeability (rock property) as follow:

$$-\frac{\partial P}{\partial L} = \frac{\mu v}{k} \qquad (1)$$

Any deviations from this linear relation (Eq. 1) may be defined as non-Darcy flow. In this study our concern is only with the non-Darcy flow caused by high fluid flow velocities. Even though Darcy's Law has been used exclusively in the studies of fluid flow in reservoirs, there is considerable evidence that high-velocity non-Darcy flow occurs in many subsurface systems, such as in the flow near wells of oil or gas production and water or gas injection. Non-Darcy flow is an important factor affecting productivity of gas wells and high-rate oil wells. In studies of non-Darcy flow through porous median, the Forchheimer equation is generally used to describe single-phase non-Darcy flow (Forchheimer, 1901). Forchheimer observed that at high flow velocities the relationship between pressure gradient and fluid velocity is no longer linear, as described by linear Darcy's flow. In an attempt to describe this nonlinear relationship, Forchheimer added an additional quadratic flow term (Eq. 2) and cubic term (Eq. 3) to the Darcy's linear form. Eq. 2 is generally known as Forchheimer's equation.

$$-\frac{\partial P}{\partial L}=\frac{\mu \mathrm{v}}{k}+\beta\rho \mathrm{v}^2 \tag{2}$$

$$-\frac{\partial P}{\partial L}=\frac{\mu \mathrm{v}}{k}+\beta\rho \mathrm{v}^2+\gamma\rho \mathrm{v}^3 \tag{3}$$

where β is the non-Darcy flow coefficient. The non-Darcy flow coefficient is usually estimated by analysis of multi-rate pressure transient tests, but such data are not always available. The usual practice to estimate values of the β factor is to use empirical correlations or theoretical equations obtained from the literature. It has been reported that β estimated from well tests is two to three times higher than β estimated from empirical correlations (Ramey, 1965; Odeh et al., 1975; Firoozabadi and Katz, 1979). There have been many correlations in the literature to estimate the non-Darcy flow coefficient. Permeability, porosity, and tortuosity are the three major parameters in the non-Darcy flow coefficient correlations.

Effects of non-Darcy or high-velocity flow regimes in porous media have been observed and investigated for decades (Tek et al., 1962; Scheidegger, 1974; Katz and Lee, 1990). The effects of non-Darcy flow on pressure transient analysis for gas wells have been investigated using numerical modeling (Smith, 1961; Swift and Kiel, 1962). The results indicated that non-Darcy flow leads to an additional pressure drop near the wellbore that may be approximated as a flow-rate-dependent skin factor. The non-Darcy flow skin factor and wellbore storage can be integrated together with the skin due to formation damage or stimulation resulting in a total skin factor as follow (Ramey, 1965):

$$S_t = S_M + Dq \tag{4}$$

where D is the non-Darcy flow coefficient and q is the production rate. This simplified approach, however, may apply in a well with a cased-hole completion, where high velocity flow occurs and converges toward perforations. This simplified approach presented in Eq. 4 may not apply to hydraulically fractured wells with non-Darcy flow in the fracture (Holditch, 1976; Guppy et al., 1982; Gidley, 1991; Settari et al., 2000). In contrast to the radial flow case, non-Darcy flow in the fracture may extend hundreds of feet away from the wellbore. The estimation of non-Darcy flow parameter, D, requires at least two different drawdown and/or buildup tests under two different constant flow rates (Ramey, 1965). Different well tests, such as flow after flow, isochronal and modified isochronal tests, have been applied to estimating the rate dependent skin factor (Cullender, 1955; Jones et al., 1975; Brar and Aziz, 1978; Kelkar, 2000). Usually multi-rate tests are not run on oil wells and therefore if non-Darcy flow is present in oil wells, it is often overlooked. Many authors have confirmed the presence of non-Darcy flow in oil wells (Fetkovich, 1973; Jones, 1975; Himmatramka, 1981; Blacker, 1982).

Many authors have observed the limitations of Forchheimer's equations to describe entire ranges of fluid velocities (Carman, 1973; Fand et al, 1987; Kececioglu and Jiang, 1994; Montillet, 2004; and Barree and Conway, 2004). In this study, we use the new flow model, proposed by Barree and Conway (2004), in the pressure transient behavior and analysis of non-Darcy flow in porous and fractured reservoirs.

The Barree and Conway model suggests using a new concept of an apparent permeability (k_{app}) to describe Darcy (linear) and non-Darcy (nonlinear) flow in porous media (Barree and Conway, 2004). The general form of this equation (Log-Dose) is given by

$$k_{app} = k_{\min} + \frac{\left(k_d - k_{\min}\right)}{\left(1+R_e^F\right)^E} \tag{5}$$

where k_{min} is the minimum permeability plateau, k_d is Darcy's permeability, F and E are constants and R_e is defined by

$$R_e = \frac{\rho \mathrm{v}}{\mu\tau} \tag{6}$$

In Eq. 6, ρ is the fluid density, v is the velocity of fluid, μ is the fluid viscosity and τ is the characteristic length which is constant for a formation system and is related to the mean particle size (Barry and Conway, 2004). The non-Darcy flow parameters in this flow model are k_{min} and τ compared to the β factor in the Forchheimer's flow model. Eq. 5 is a generic equation that describes data exhibiting a power law slope bounded by two plateau regions. The Forchheimer equation can be written as

$$\frac{\partial P}{\partial L}=\frac{\mu \mathrm{v}}{k_d}\left(1+\frac{\beta k_d \rho \mathrm{v}}{\mu}\right) \tag{7}$$

Eq. 7 can be further simplified as

$$\frac{\partial P}{\partial L} = \frac{\mu \mathrm{v}}{k_{app}} \tag{8}$$

where

$$k_{app} = \frac{k_d}{\left(1 + R_p\right)} \tag{9}$$

$$R_p = \frac{\beta k_d \rho \mathrm{v}}{\mu} \tag{10}$$

In Eq. 5, if the two exponents E and F are set to 1.0 and the value of k_{min} is set to zero, the general form (Eq. 5) reduces to the form of Eq. 9 which is re-statement of the Forchheimer equation (Eq. 2). Assuming the values of the exponents E and F are 1.0 and using a minimum permeability divided (or relative to) the Darcy permeability, Eq. 5 becomes

$$k_{app} = k_d \left(k_{mr} + \frac{\left(1 - k_{mr}\right)}{\left(1 + \rho \mathrm{v} / \mu\tau\right)} \right) \tag{11}$$

where

$$k_{mr} = \frac{k_{\min}}{k_d} \tag{12}$$

The form of the apparent permeability given by Eq. 11 is very powerful since it can describe any flow system. By substituting Eq. 11 in Eq. 8, the complete nonlinear flow model for non-Darcy 1-D flow following the Barree and Conway model (Barree and Conway, 2004) is given by

$$\frac{\partial P}{\partial L} = \frac{\mu \mathrm{v}}{k_d \left(k_{mr} + \frac{\left(1 - k_{mr}\right)}{\left(1 + \rho \mathrm{v} / \mu\tau\right)} \right)} \tag{13}$$

The Barree and Conway model can be extended to multidimensional fluid flow as follow

$$-\nabla\Phi = \frac{\mu \mathbf{v}}{k_d \left(k_{mr} + \frac{\left(1 - k_{mr}\right)\mu\tau}{\mu\tau + \rho|\mathbf{v}|} \right)} \tag{14}$$

where $\mathbf{v}$ is the flow velocity vector and the flow potential gradient $\nabla\Phi$ is given by

$$\nabla\Phi = \left(\nabla P_\beta - \rho_\beta \, g \, \nabla D\right) \tag{15}$$

where P_β is the pressure of phase β, g is gravitational acceleration and D is depth. Eq. 14 represents the mathematical model used in this study for the Barree and Conway flow model.

Researchers showed experimentally on proppant packs that the new flow model developed by Barree and Conway can describe all fluid velocities ranges accounting for nonlinear non-Darcy flow (Lai et al., 2009). However, the flow model developed by Barree and Conway has not been used yet to analyze pressure-transient well tests with non-Darcy flow effects. In this paper we investigate applying this new flow model to well testing pressure-transient applications for single-phase non-Darcy flow behavior in porous and fractured reservoirs.

Mathematical Model

Consider the flow of a single fluid (single component or a homogenous mixture) through a small control volume of an arbitrary shape within the porous medium, the law of conservation of mass states that the difference between inflow and outflow must be equal to the sum of accumulation of mass within the control volume. For fluid flow of a single phase β (oil or gas) in porous media, the conversation of mass or continuity equation is given by

$$\frac{\partial}{\partial t}\left(\phi\,\rho_\beta\right) = -\nabla \bullet \left(\dot{\boldsymbol{m}}_\beta\right) + q_\beta \tag{16}$$

where ϕ is the effective porosity of formation, ρ_β is the density of phase β at reservoir conditions, m_β is mass flux of the fluid and q_β is the sink/source term of component β per unit volume of formation. The mass flux of the fluid can be expressed in terms of superficial velocity as follow

$$\dot{\boldsymbol{m}}_\beta = \rho_\beta\,\mathbf{v}_\beta \tag{17}$$

Combining Eqs. 16 and 17 we obtain the following fluid flow (continuity) equation:

$$\frac{\partial}{\partial t}\left(\phi\,\rho_\beta\right) = -\nabla \bullet \left(\rho_\beta\,\mathbf{v}_\beta\right) + q_\beta \tag{18}$$

Eq. 18 is a general governing equation that describes the flow of a single-phase fluid in reservoirs. The divergence operator on the first term of the right-hand side of Eq. 18 may be expanded in any reservoir coordinate system. For example, for a three-dimensional fluid flow in a Cartesian system of coordinates (x, y, z) Eq. 18 becomes

$$\frac{\partial}{\partial t}\left(\phi\,\rho_\beta\right) = -\left(\frac{\partial}{\partial x}\rho_\beta\,\mathrm{v}_x + \frac{\partial}{\partial y}\rho_\beta\,\mathrm{v}_y + \frac{\partial}{\partial z}\rho_\beta\,\mathrm{v}_z\right) + q_\beta \tag{19}$$

For a three-dimensional fluid flow in a cylindrical coordinates (r, θ, z) Eq. 18 becomes

$$\frac{\partial}{\partial t}\left(\phi\,\rho_\beta\right) = -\left(\frac{1}{r}\frac{\partial}{\partial r}\rho_\beta\,r\,\mathrm{v}_r + \frac{1}{r}\frac{\partial}{\partial \theta}\rho_\beta\,\mathrm{v}_\theta + \frac{\partial}{\partial z}\rho_\beta\,\mathrm{v}_z\right) + q_\beta \tag{20}$$

Well testing applications assume fluid flow in one- or two-dimensional radial system of coordinates (r, z). Eq. 18 for a 2-D radial reservoir system is

$$\frac{\partial}{\partial t}\left(\phi\,\rho_\beta\right) = -\left(\frac{1}{r}\frac{\partial}{\partial r}\rho_\beta\,r\,\mathrm{v}_r + \frac{\partial}{\partial z}\rho_\beta\,\mathrm{v}_z\right) + q_\beta \tag{21}$$

In addition to the equation of continuity or mass conservation (Eq. 18), we require a relationship between the fluid velocity and the pressure gradient. For non-Darcy flow using the Barree and Conway model, the velocity of phase β is defined as

$$\mathrm{v} = \frac{-\left(\mu^2\tau - k_d k_{mr}\rho\frac{\partial P}{\partial L}\right) + \sqrt{\left(\mu^2\tau - k_d k_{mr}\rho\frac{\partial P}{\partial L}\right)^2 + 4\mu^2\rho k_d\tau\frac{\partial P}{\partial L}}}{2\mu\rho} \tag{22}$$

Eq. 22 is obtained by solving Eq. 13 (Barree and Conway model) for the velocity.

Numerical Model

The numerical technique used in numerical simulation of fluid flow in porous and fractured reservoirs is the "integral finite difference" method (Narasimhan and Witherspoon, 1976; Pruess, 1999). The mass balance equations for fluids are expressed in terms of a set of discrete integral finite difference equations. These discrete non-linear equations are then solved either fully implicitly to provide stability and large time step size or using the AIM (Adaptive Implicit Method) to speed up simulation times and reduce space storage requirement. Thermodynamic properties of fluids and rock are represented by averages over explicitly defined finite subdomains or grid blocks, while fluxes of mass across surface segments between

connected grid blocks are evaluated by finite difference approximations. The discretized, non-linear, finite difference mass-balance equations are then solved simultaneously, using the Newton/Raphson iteration procedure.

Numerical Discretization

In this study, the numerical approach to simulate the non-Darcy flow consists of spatial discretization of the mass conservation equation, time discretization; and iterative approaches to solve the resulting nonlinear, discrete algebraic equations. A mass-conserving discretization scheme, based on control-volume or integral finite-difference, IFD, (Pruess et al. 1999) is used. The control-volume approach provides a general spatial discretization scheme that can represent a one-, two- or three-dimensional domain using a set of discrete meshes. Time discretization is carried out using a backward, first-order, fully implicit finite-difference scheme.

Eq. 18 discretized in space using an integral finite-difference or control-volume scheme for a porous and/or fractured medium with an unstructured grid as shown in Figure 1. The time discretization is carried out with a backward, first-order finite difference method. Then the discrete non-linear equations of element i are as follows.

$$\left\{\left(\phi\,\rho_\beta\right)_i^{n+1}-\left(\phi\,\rho_\beta\right)_i^{n}\right\}\frac{V_i}{\Delta t}=\sum_{j\in\eta_i}F_{ij}^{n+1}+Q_{\beta i}^{n+1} \tag{23}$$

where n denotes the previous time level, $n+1$ is the current time level, V_i is the volume of element i (porous or fractured block), Δt is the time step size, η_i contains the set of neighboring elements (j) (porous or fractured) to which element i is directly connected, Q_i is the mass sink/source term at element i, for the fluid and is defined as

$$Q_{\beta i}^{n+1}=q_{\beta i}^{n+1}V_i \tag{24}$$

and F_{ij}^{n+1} is the mass "flow" term for the fluid between elements i and j. Eq. 23 is a discrete equation of mass conservation of the fluid, has the same form regardless of the dimensionality of the model domain, i.e., it applies to one-, two-, or three-dimensional flow through porous or fractured media (Wu, 2002).

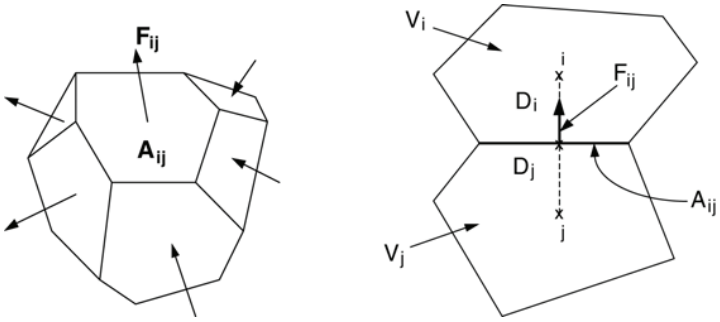

Figure 1 – Space discretization and flow-term evaluation in the IFD method (Pruess et al. 1999)

Using the Barree and Conway flow model to simulate the non-Darcy flow behavior then, based on Eq. 14, the mass flow term for the fluid between elements i and j is defined as

$$F_{ij}=\frac{A_{ij}}{2\mu}\left[-(\mu^2\tau-\left(k_d k_{mr}\rho\right)_{ij+1/2}\left[\frac{\left(\Phi_j-\Phi_i\right)}{d_i+d_j}\right])+\sqrt{\left(\mu^2\tau-\left(k_d k_{mr}\rho\right)_{ij+1/2}\left[\frac{\left(\Phi_j-\Phi_i\right)}{d_i+d_j}\right]\right)^2+4\mu^2\left(\rho k_d\right)_{ij+1/2}\tau\left[\frac{\left(\Phi_j-\Phi_i\right)}{d_i+d_j}\right]}\right] \tag{25}$$

where subscript ij+1/2 denotes a proper averaging or weighting of properties at the interface between the two elements i and j, A_{ij} is the common interface area between the connected blocks or nodes i and j, μ is the viscosity of the fluid, ρ is the density of the fluid, d_i is the distance from the center of block i to the common interface of blocks i and j, τ is the characteristic length, k_d is Darcy's permeability, k_{mr} is the ratio of minimum permeability plateau to Darcy's permeability (Eq. 12) and Φ is the flow potential term and defined by Eq. 15.

Numerical Solution Method

Eq. 23 (discretized/nonlinear continuity equation) is solved fully implicitly using a Newton-Raphson iteration method. The discrete nonlinear equation (Eq. 23) can be written in a residual form as follow:

$$R_i = \left\{ (\phi \ \rho)_i^{n+1} - (\phi \ \rho)_i^n \right\} \frac{V_i}{\Delta t} - \sum_{j \in \eta_i} F_{ij}^{n+1} - Q_i^{n+1} \qquad \{i = 1, 2, 3, ..., N\} \tag{26}$$

where N is the total number of nodes, elements or grid blocks of the grid system. Eq. 26 defines a set of (N) coupled nonlinear mass balance equations that need to be solved simultaneously. One primary variable per node is needed to use in the Newton-Raphson iteration for solving one equation per node. The fluid pressure is selected as the primary variable, and treats all the rest of the dependent variables, such as viscosity, porosity, and density as secondary variables, which are calculated from the primary variable at each node and at each iteration. In terms of the primary variable, the residual equation, Eq. 26, at a node i is regarded as a function of the primary variables at not only node i, but also at all its directly neighboring nodes j. Applying Newton-Raphson iteration scheme gives:

$$\frac{\partial R_i^{n+1}(x_{j,p})}{\partial x_j} (\delta x_{i,p+1}) = -R_i^{n+1}(x_{m,p}) \qquad \{i = 1, 2, 3, ..., N\} \tag{27}$$

where x_j is the primary variable at node i and all its direct neighbors; p is the iteration level. The primary variables in Eq. 27 need to be updated after each iteration as shown by Eq. 28:

$$x_{p+1} = x_p + \delta x_{p+1} \tag{28}$$

The Newton-Raphson iteration process continues until the residuals, $R_i^{k,n+1}$, or changes in the primary variables, δx_{p+1}, over an iteration are reduced below preset convergence tolerances. In addition, the numerical method is used to construct the Jacobian matrix for Eq. 27, as outlined in Forsyth et al. (1995). At each Newton-Raphson iteration, Eq. 27 represents a system of N linearized algebraic equations with sparse matrices, which are solved by a linear iterative matrix equation solver. The matrix solution used in numerical simulator uses the modern sparse technique-matrix solver. The linear-equation solution technique is the advanced state-of-the-art of sparse matrix solver, which is based on an incomplete LU factorization (ILU) with CG-like acceleration schemes (Clift et al., 1996). The robustness and efficiency of the numerical solution scheme have been tested in many simulations from theoretic studies to field applications (Wu, 2000).

Treatment of Initial and Boundary Conditions

Similarly to Darcy flow, first-type or Dirichlet boundary conditions can be treated using the large-volume or inactive-node method (Pruess, 1999), in which a constant pressure node may be specified with a huge volume while keeping all the other geometric properties of the mesh unchanged. Once specified, primary variables will be fixed at the big-volume boundary nodes, and the code handles these boundary nodes exactly like any other computational nodes. Flux-type or Neuman boundary conditions are treated as sink/source terms, depending on the pumping (production) or injection condition, which can be directly added to Eq. 26. This treatment of flux-type boundary conditions is especially useful for a situation where flux distribution along the boundary is known, such as dealing with a single-node well. More general treatment of multilayered well-boundary conditions is discussed in Wu et al. (1996 and 2000).

Handling Non-Darcy Flow in Fractured Reservoirs

Understanding and modeling fracture flow phenomena in porous media have been observed and studied for decades (e.g., Barenblatt et al., 1960; Warren and Root, 1963; Kazemi, 1969; Pruess and Narasimhan, 1985). Warren and Root (1963) has developed the classical double-porosity concept for modeling flow in fractured porous media that assumes a flow domain is composed of matrix blocks of low permeability embedded in a network of interconnected more permeable fractures. Global flow in the formation occurs only through the fracture system, described as an effective porous continuum. The matrix behaves as spatially distributed sinks or sources to the fracture system without accounting for global matrix-matrix flow. If a global matrix-matrix flow is included, the approach becomes a dual-permeability conceptual model. The double-porosity or dual-permeability model relies on a quasi-steady-state flow assumption to account for fracture-matrix interflow. This may limit their applicability in application to situations having only matrix blocks of small size to satisfy the quasi-steady state mass transfer condition. The generalized dual-continuum method, such as the MINC concept (Pruess and Narasimhan, 1985) and the multiporosity model (Wu and Pruess, 1988), can describe flow in a fracture/matrix system with any size and shape of matrix blocks and with fully transient handling of fracture/matrix interactions. The generalized dual-continuum, MINC method, can handle any flow processes of fractured media with matrix size varying from as large as the model domain of interest to as small as a representative elementary volume (REV). In general, the fracture network can be continuous in a pattern, randomly distributed or discrete.

The technique used in the numerical model of this study for handling non-Darcy flow through fractured rock follows the dual-continuum methodology (Warren and Root, 1963; Pruess, 1991; Pruess and Narasimhan, 1985). The method treats fracture and matrix flow and interactions using a multi-continuum numerical approach, including the double- or multiporosity method (Wu and Pruess, 1988), the dual-permeability method, and the more general "multiple interacting continua" (MINC) method

(Pruess and Narasimhan, 1985). The non-Darcy flow formulation (Eqs. 16, 23 and 25) is applicable to both single-continuum and multi-continua media. Using the dual-continuum concept, Eqs. 16, 23 and 25 can be used to describe single-phase flow both in fractures and inside matrix blocks when dealing with fractured reservoirs. A special attention needs to be paid to treating fracture/matrix flow terms with Eq. 23 for estimation of mass exchange at fracture/matrix interfaces using a double-porosity approach. Eq. 25 that describes flow according to Barree and Conway model is used for calculations of flow between matrix and fracture. However, k_d and k_{min} parameters used in Eq. 25 are only for the matrix and no averaging is required. The characteristic length of non-Darcy flow distance between fractures and matrix crossing the interface for the double-porosity or the nested discretization may be approximated using the results for Darcy flow (Warren and Root, 1965; Pruess, 1983). When handling flow through a fractured rock using the numerical formulation of this work, the problem essentially becomes how to generate a mesh that represents both the fracture and matrix systems. Several fracture-matrix sub-gridding schemes exist for designing different meshes for different fracture-matrix conceptual models (Pruess, 1983). Once a proper mesh of a fracture-matrix system is generated, fracture and matrix blocks are specified to represent fracture or matrix domains, separately.

Numerical Simulation of Skin Zone

An example of how to simulate the skin zone for a radial reservoir in non-Darcy flow numerical models is shown in Figure 2. The skin zone (damaged or stimulated) can be numerically simulated by at least two control volume elements.

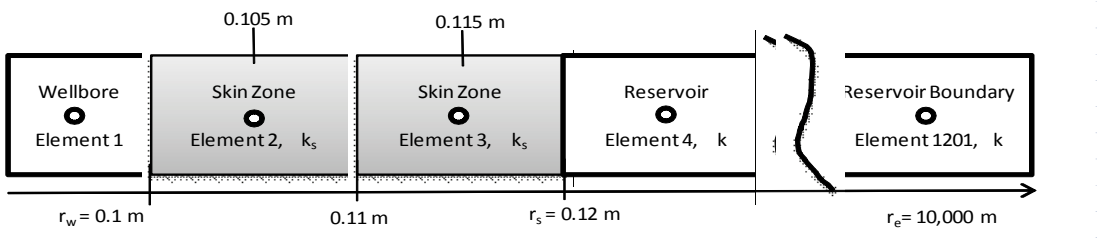

Figure 2 – Illustration example of how to simulate the skin zone in the numerical model

For a given value of skin factor (S), wellbore radius (r_w), and reservoir permeability (k); the permeability of the skin zone (k_s) is calculated using the following equation for any skin zone radius (r_s) (Hawkins, 1956):

$$k_s = k \Big/ \left(\frac{S}{Ln(r_s/r_w)} + 1 \right) \tag{29}$$

Then, the calculated skin zone permeability (Eq. 29) is input to the numerical simulator as a rock property for the two control elements. The mesh section in the simulator generates the grid data for the given reservoir system. It is flexible in the numerical simulator to change the skin zone radius by controlling the elements in the generated mesh or gird. Following the strategy above, the data shown in Table 1 was used to generate synthetic pressure transient responses for different skin factors (S = 0, 1, 5 and 10) using the Barree and Conway flow numerical model ($k_d = k_{min}$ = 100 md, no non-Darcy effects). Then the simulation results were compared to the analytical solution as shown in Figure 3. An excellent agreement was obtained between the numerical model and the analytical solution for all values of skin factors.

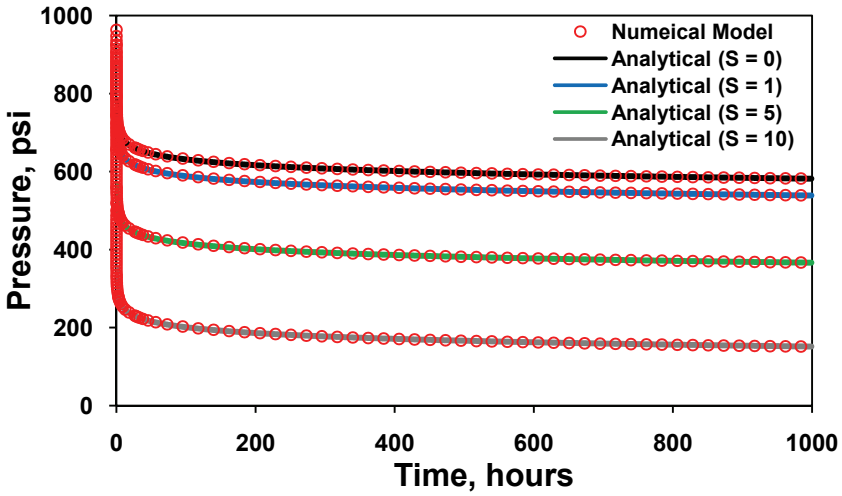

Figure 3 – Comparison of numerical and analytical solutions for different skin factors using Barree and Conway model

Table 1 - Input data used for comparison of analytical and numerical (Barree and Conway model) solutions for different values of skin factor (S) and wellbore-storage coefficient (C)

Parameter	Value	Unit
Darcy Permeability	k_d = 100	md
Minimum Permeability	k_{min} = 100	md
Skin Factor	S = 0, 1, 5, 10	
Wellbore Storage Coefficient	C = 0, 0.05, 0.5, 1	bbl/psi
Viscosity	μ = 1	cp
Porosity	ϕ = 0.2	
Density	ρ = 60	lb/ft3
Total Compressibility	$C_t = 10x10^{-6}$	psi^{-1}
Production Rate	q = 1,000	bbl/d
Formation Thickness	h = 32.81	ft
Initial Pressure	P_i = 1,000	psi
Reservoir drainage radius	r_e = 32,810	ft
Wellbore Radius	r_w = 0.3281	ft

Numerical Simulation of Wellbore Storage

If the production rate is constant at surface condition, then the wellbore storage effect may last for a period of time, depending on the wellbore store volume and the rate of unloading the produced fluid. In drawdown tests the fluid stored in the wellbore after shut-in period will unload from the wellbore with no flow from the reservoir to the wellbore. At time passes, the flow rate (from reservoir to wellbore) will equal to the surface production rate with the amount of fluid stored being constant. The wellbore storage coefficient (C) may be defined as the ability of the wellbore to store or unload fluid per unit change in pressure and it depends on the situation in the wellbore. During that short time of wellbore store (buildup) or unload (drawdown) fluids, the transient pressure response is not the true reservoir response to be analyzed for formation properties. In single-phase fluid flow the wellbore storage coefficient (C, bbl/psi) may be defined as

$$C = V_{wb} c_{wb} \tag{30}$$

where V_{bw} is the volume of the wellbore in bbl and c_{wb} is the compressibility of the wellbore fluid in psi^{-1}. In numerical simulator we compute V_{wb} for a given value of C and c_{wb}. Since the numerical simulator considers the well element as a "reservoir" element by multiplying it by the porosity of the matrix, then we must divided the computed volume, V_{wb}, by the porosity to consider all the volume of the wellbore as follow

$$V_{wb-element} = \frac{C}{\phi c_{wb}} \tag{31}$$

Then this computed volume, $V_{wb\text{-}element}$, is input to the numerical model as the volume of the well element in the reservoir grid system to actually represent physically the wellbore.

The data, shown in Table 1, were used to generate synthetic pressure transient responses for different wellbore storage coefficients (C = 0, 0.05, 0.5 and 1 bbl/psi) using the Barree and Conway flow numerical model ($k_d = k_{min}$ = 100 md, no non-Darcy effects). The simulation results were compared to the analytical solution as shown in Figure 4. An excellent agreement was obtained between the numerical model and the analytical solution for all values of wellbore storage coefficients.

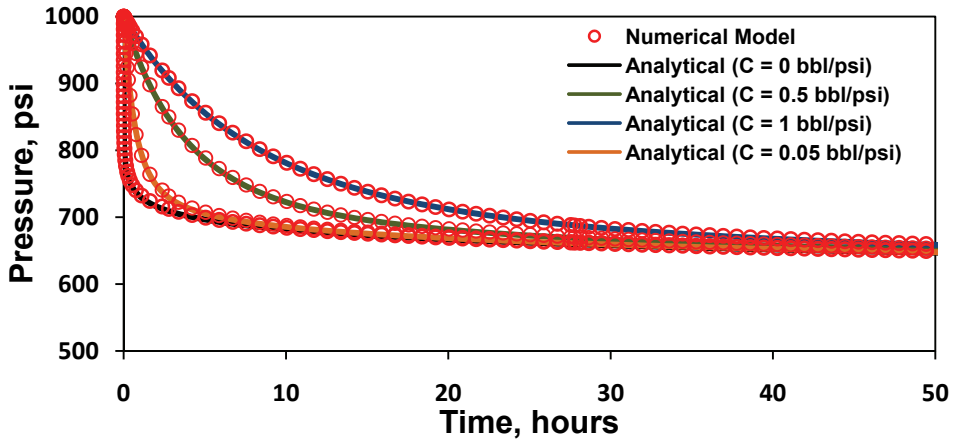

Figure 4 – Comparison of numerical and analytical solutions for different wellbore-storage, C, using Barree and Conway model

Verification of Numerical Model

An analytical steady-state flow solution of a 1-D radial reservoir for incompressible, slightly compressible and compressible fluids according to the Barree and Conway model is derived. Appendix A presents the derivations in details. The analytical solution is here used to check the numerical model. The analytical steady-state solution of 1-D radial reservoir for incompressible fluid according to the Barree and Conway model is given by

$$P = P_i - \frac{1}{k_d \rho_i}\left[\frac{\mu \dot{m}}{2\pi h k_{mr}}\left\{\ln\left(\frac{r_e}{r}\right) - \left(k_{mr} - 1\right)\ln\left(\frac{\dot{m}k_{mr} + \left(2\pi h \mu\tau\right)r_e}{\dot{m}k_{mr} + \left(2\pi h \mu\tau\right)r}\right)\right\}\right] \tag{32}$$

In numerical simulation, the porous formation is assumed uniform, radially finite of 100 ft thick and is represented by a radially-symmetrical, cylindrical reservoir (RxZ, 10,000x100 ft), discretized into a one-dimensional (R), the r-distance of 10,000 ft is subdivided into 310 intervals (volume elements) in logarithmic scale with a Δr size that increases logarithmically away from the wellbore (r_w = 0.3 ft). The formation is initially at a constant pressure of 5,000 psi and is subjected to a constant production rate of 2,500 reservoir bbl/day at the producing well, starting at time of zero. The input parameters used for the numerical simulation are listed in Table 2. The pressure at the outlet boundary is maintained at the initial pressure (5,000 psi), and a constant mass production rate (2,500 bbl/day) is proposed at the wellbore (r_w = 0.3 ft) for both the analytical and numerical solutions. The numerical calculations are carried out until steady state is reached. Several simulation cases where run to check consistency of numerical model and the analytical solution. The Barree and Conway model, non-Darcy flow, parameters used are the characteristic length, τ, and the minimum permeability plateau, k_{min}. The first comparison case was run for two values of the characteristic length (τ = 1,000 and 0.001 (1/ft)). Figure 5 presents a comparison between the analytical and numerical solutions for this case. Figure 5 indicates that excellent results are obtained from the numerical simulation, as compared to the analytical solution.

Table 2 - Input data used for comparison of analytical and numerical (Barree and Conway model) solutions

Parameter	Value	Unit
Darcy Permeability	k_d = 100	md
Minimum Permeability	k_{min} = 25, 50, 100	md
Characteristic Length	$\tau = 10^{-3}, 10^{3}$	1/ft
Porosity	ϕ = 0.2	
Viscosity	μ = 1	cp
Density	ρ = 60	lb/ft3
Production Rate	q = 2,500	bbl/day
Formation Thickness	h = 100	ft
Pressure at outer boundary	P_i = 5,000	psi
Reservoir drainage radius	r_e = 10,000	ft
Wellbore Radius	r_w = 0.3	ft

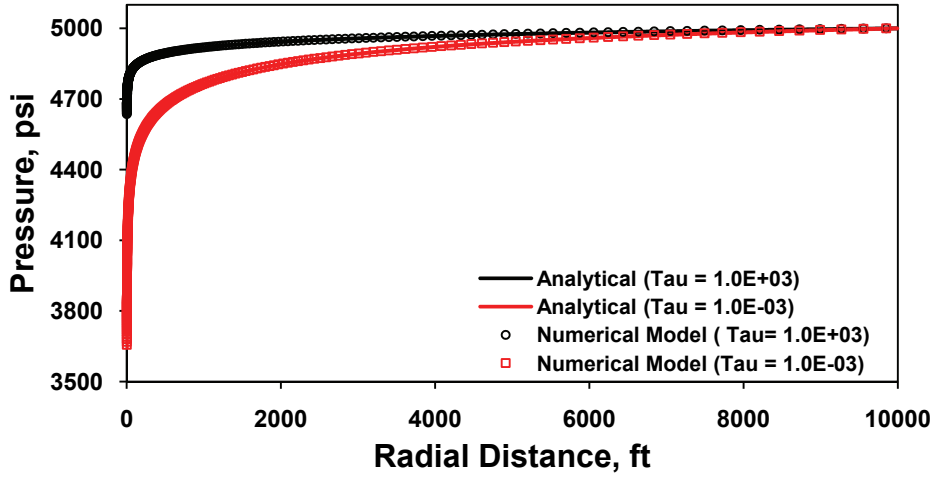

Figure 5 – Comparison of analytical and numerical solutions for steady-state radial flow and for two different values of the characteristic length using Barree and Conway model

The second comparison case was run for three values of the minimum permeability plateau (k_{min} = 25, 50 and 100 md). Figure 6 presents a comparison between the analytical and numerical solutions for this case. Figure 6 indicates that excellent results are obtained from the numerical simulation, as compared to the analytical solution.

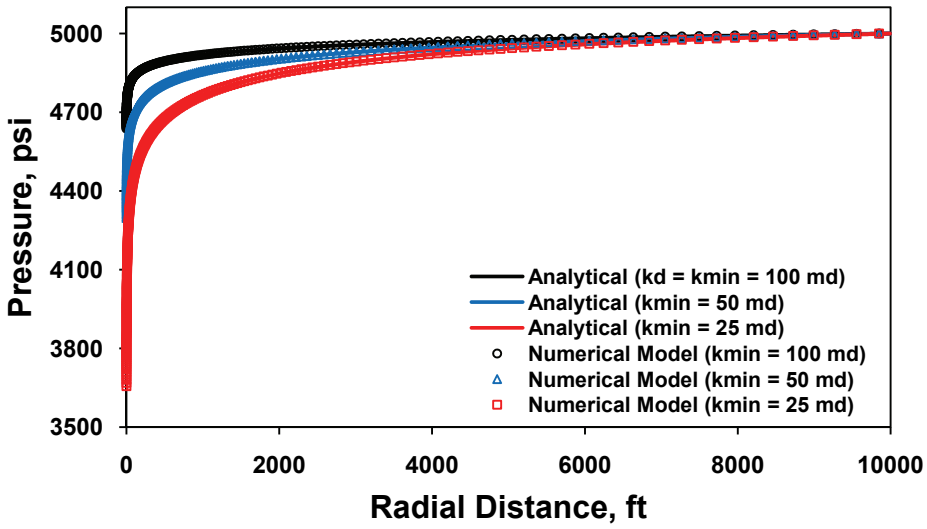

Figure 6 – Comparison of analytical and numerical solutions for steady-state radial flow and for three different values of the minimum permeability plateau using Barree and Conway model

Examples and Field Applications

This section shows synthetic examples, type-curves from the numerical model and field applications (actual well testing data) of using the developed non-Darcy numerical model according to the Barree and Conway flow model to interpret and analyze pressure drawdown and buildup tests in porous reservoirs.

Transient-Pressure Type Curves

This example shows type curves generated from transient non-Darcy flow model incorporating the Barree and Conway model. These type curves can be used to match actual pressure-transient data and analyze combined effects of non-Darcy flow behavior, skin effect and wellbore storage by curve-fitting. The dimensionless pressure, time, wellbore-storage and skin factor are defined by Eqs. 33-36 for constant production in a radial reservoir.

$$P_D = \frac{k_d\ h}{141.2\ q\ \beta\ \mu}\left(P_i - P\right) \tag{33}$$

$$t_D = \frac{0.0002637\ k_d\ t}{\phi\ \mu\ c_t\ r_w^2} \tag{34}$$

$$C_D = \frac{0.8936\ C}{\phi\ c_t\ h\ r_w^2} \tag{35}$$

$$S = \frac{k_d\ h\ \Delta P_s}{141.2\ q\ \beta\ \mu} \tag{36}$$

The dimensionless non-Darcy flow parameter, k_{mr}, according to Barree and Conway is defined as:

$$k_{mr} = \frac{k_{\min}}{k_d} \tag{37}$$

The dimensionless non-Darcy flow parameter, τ_D, is defined based on distance in radial-direction as:

$$\tau_D = \frac{\tau}{r} \tag{38}$$

In Eq. 38, if we analyze pressure-transient data for wellbore pressure, as the case of this example, then $r = r_w$. Input data used for generating pressure transient type-curves in this example are listed in Table 3. In numerical simulation, the porous reservoir system is assumed uniform, radially finite of 100 ft thick and is represented by a 1-D radial grid of 2,010 volume elements with a Δr size that increases logarithmically away from the wellbore (r_w = 0.3 ft). Figures 7 and 8 show example type-curves generated from the numerical model studying effect of non-Darcy flow parameters (k_{mr} and τ_D) according to Barree and Conway model with combined effect of skin (S = 1) and wellbore storage (C_D = 500). Figure 7 shows log-log plot of dimensionless pressure versus dimensionless time for different values of dimensionless non-Darcy flow parameter k_{mr} (1, 0.5 and 0.2) with a fixed value of τ_D of 0.1, skin factor of 1.0 and C_D of 500. The early time, unit-slope, straight line indicates clearly the effect of wellbore storage. The value of k_{mr} of 1.0 is simulating Darcy's flow with skin factor of 1.0. Note that the generated type-curves combine both effects of skin (damage in this example) and non-Darcy flow. As the value of k_{mr} decreases we can see clearly more increase in pressure drop due to non-Darcy flow. Figure 8 shows type curve (log-log plot of p_D versus t_D) for different values of dimensionless non-Darcy flow parameter τ_D (0.01, 10, 1000) with fixed value of k_{mr} of 0.5, skin factor of 1.0 and C_D of 500. As the value of τ_D decreases we can notice the increase in pressure drop due to non-Darcy flow. However this increase in pressure drop is less than the effect of decreasing k_{mr} (see Figure 7). In actual cases we expect low values of the characteristic length, τ, thus the major contributing parameter of non-Darcy flow according to the Barree and Conway model, in this example, is the minimum permeability plateau, k_{min}.

Table 3 - Input data used for generating type-curves of transient non-Darcy flow using Barree and Conway model

Parameter	Value	Unit
Minimum Permeability relative to Darcy's Permeability	k_{mr} = 1, 0.5, 0.2	
Dimensionless Characteristic Length	τ_D = 0.1, 10, 100	
Dimensionless Wellbore-Storage	C_D = 500	
Skin Factor	S = 1	
Porosity	ϕ = 0.2	
Viscosity	μ = 1	cp
Density	ρ = 60	lb/ft3
Formation Thickness	h = 100	ft
Pressure at outer boundary	P_i = 5,000	psi
Reservoir drainage radius	r_e = 10,000	ft
Total Compressibility	$c_t = 10x10^{-6}$	psi^{-1}
Production Rate	q = 5,000	bbl/day
Wellbore Radius	r_w = 0.3	ft

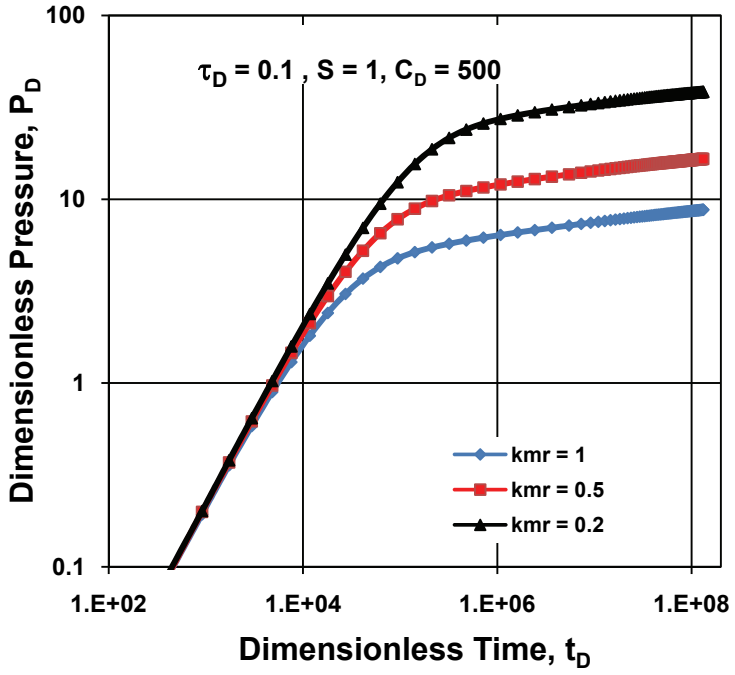

Figure 7 – Type curves of transient non-Darcy flow using Barree and Conway model showing effect of non-Darcy flow parameter k_{mr}

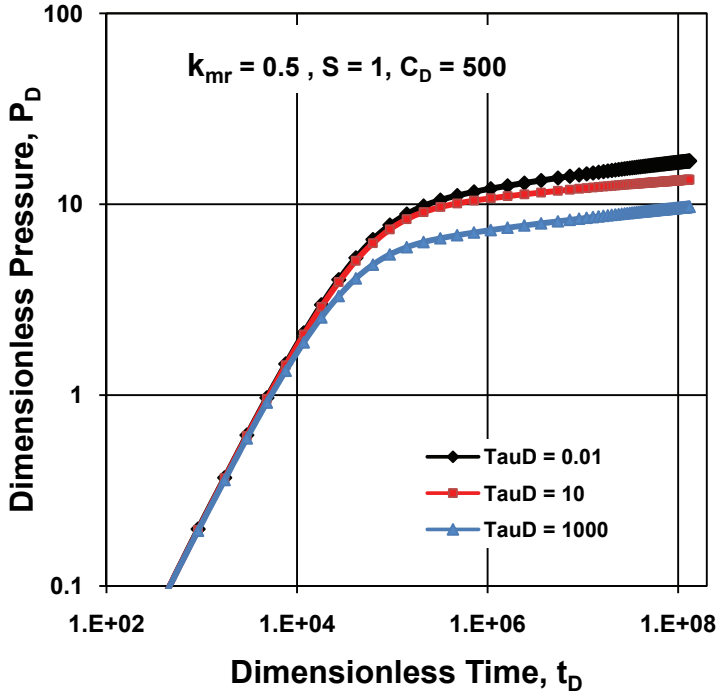

Figure 8 – Type curves of transient non-Darcy flow using Barree and Conway model showing effect of non-Darcy flow parameter τ_D

Pressure Drawdown Tests in Reservoirs

This example shows a pressure drawdown test in a porous-medium reservoir rock using the non-Darcy simulation model according to the Barree and Conway flow model. Synthetic pressure transient responses are generated from the numerical model to study effects of the non-Darcy flow parameters of the Barree and Conway model. The near wellbore effects, such as skin and/or wellbore storage effects, have not been considered in these simulation cases for unaffected pressure responses while studying effects of non-Darcy flow parameters. In the numerical model, the porous-medium reservoir system is assumed uniform, radially finite of 100 ft thick and is represented by a 1-D radial grid of 2,010 volume elements with a Δr size that increases logarithmically away from the wellbore (r_w = 0.3 ft). The formation is initially at a constant pressure of 5,000 psi and is subjected to a constant production rate of 5,000 bbl/day at the producing well, starting at time of zero. Input data used for simulating the pressure transient responses in the numerical model are listed in Table 4.

Table 4 - Input parameters used for numerical simulation of pressure transient responses of non-Darcy flow using Barree and Conway model for pressure drawdown test example in porous radial reservoir

Parameter	Value	Unit
Darcy Permeability	k_d = 100	md
Minimum Permeability	k_{min} = 25, 50, 75, 100	md
Characteristic Length	$\tau = 10^{-6}, 10^{-3}, 10^{-1}, 1, 10, 10^{2}, 10^{3}, 10^{6}$	1/ft
Porosity	ϕ = 0.2	
Viscosity	μ = 1	cp
Density	ρ = 60	lb/ft3
Production Rate	q = 1000, 2500, 5000	bbl/day
Formation Thickness	h = 100	ft
Pressure at outer boundary	P_i = 5,000	psi
Reservoir drainage radius	r_e = 10,000	ft
Total Compressibility	$c_t = 10x10^{-6}$	psi^{-1}
Wellbore Radius	r_w = 0.3	ft

Effect of Minimum Permeability

Several simulation cases were run using the numerical model to see the effect of the minimum permeability, k_{min}, on the non-Darcy pressure transient responses during a pressure drawdown test. The input data in Table 4 was used with a fixed value of characteristic length, τ, of 1 (1/ft) and a constant production rate of 5,000 bbl/day. Figure 9 presents the simulated pressure transient responses at the producing well. The pressure drop due to the non-Darcy flow effects increases as the value of minimum permeability decreases, showing a very high non-Darcy flow effects when k_{min} parameter is very low (Case of k_{min} = 25 md). Increasing the value of k_{min} parameter reduces non-Darcy pressure drop showing a Darcy's flow behavior when k_{min} parameter is very high and equals to the constant Darcy's permeability (Case of $k_{min} = k_d$ = 100 md).

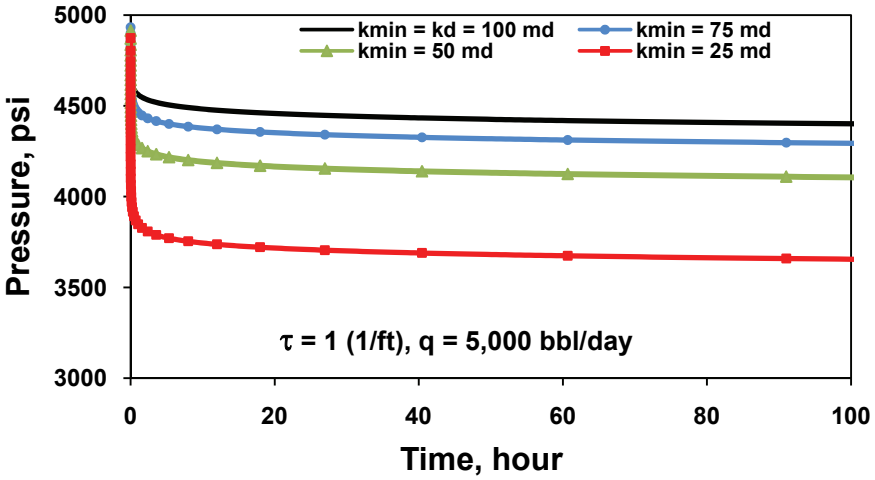

Figure 9 – Effect of non-Darcy flow minimum permeability, k_{min}, on the pressure transient responses of a pressure drawdown test example in a porous radial reservoir using Barree and Conway model

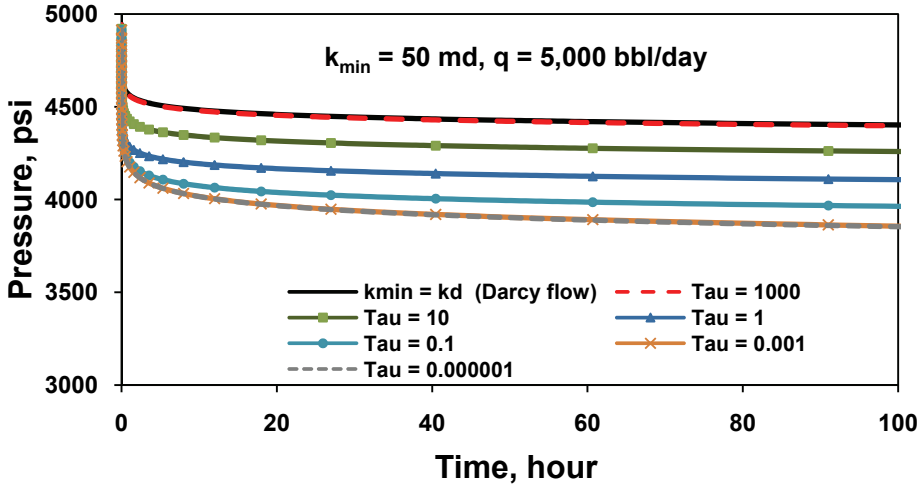

Figure 10 – Effect of non-Darcy flow characteristic length, τ, on transient responses of pressure drawdown test example in porous radial reservoir using Barree and Conway model

Effect of Characteristic Length

Sensitivity cases were run to investigate the effect of the characteristic length, τ, on the non-Darcy pressure transient responses of a pressure drawdown test. The input data in Table 4 was used with a fixed value of minimum permeability, k_{min}, of 50 md and a constant production rate of 5,000 bbl/day. The reason for choosing a k_{min} case of 50 md is because it shows a non-Darcy pressure drop ranges between minimum value at k_d = 100 md and maximum value at k_{min} = 25 md (see Figure 9). Figure 10 presents the simulation results. The pressure drop due to the non-Darcy flow increases as the value of the characteristic length decreases, showing a very high non-Darcy or nonlinear flow effects when the value of τ is very low (less than or equal 0.001 (1/ft) in this example, see Figure 10). Increasing the value of the characteristic length reduces the non-Darcy or nonlinear flow behavior up to a maximum value (1,000 (1/ft) in this example, see Figure 10) where the flow becomes mainly Darcy's linear flow.

Effect of Production Rate

The non-Darcy flow behavior is more sensitive to the production rate. At higher production rates we expect more significant pressure drop due to the stronger non-Darcy flow behavior. Several cases were run changing the well production rate to investigate the impact of the non-Darcy flow parameters (k_{min} and τ) on the pressure transient responses of the pressure drawdown test. Sensitivity cases were run from high production rate of 5,000 bbl/day to low value of 1,000 bbl/day. For production rates below 1,000 bbl/day, the non-Darcy flow behavior becomes insignificant. Figures 11 and 12 represent the simulated non-Darcy pressure responses for a production rate of 1,000 bbl/day. The same as concluded previously, both the minimum permeability plateau and the characteristic length parameters are sensitive and affect the pressure transient responses. Since changing one flow parameter requires setting the other parameter constant in the simulation runs, we found that the characteristic length is more sensitive compared to the minimum permeability plateau especially at low production

rates. If a higher value of the characteristic length is used (minimizing the non-Darcy flow behavior toward Darcy's flow) then changing the minimum permeability plateau value (even to a very low value, maximizing the non-Darcy flow behavior) will not affect the pressure transient responses.

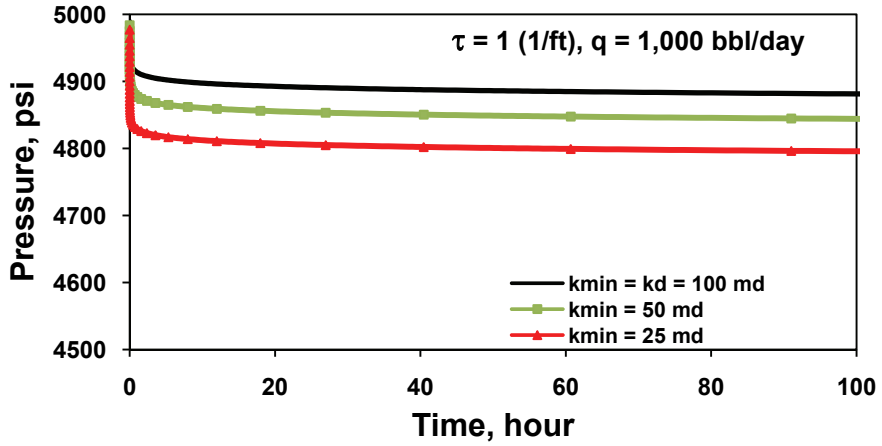

Figure 11 – Effect of non-Darcy flow minimum permeability, k_{min}, and low production rate on transient responses of pressure drawdown test example using Barree and Conway model

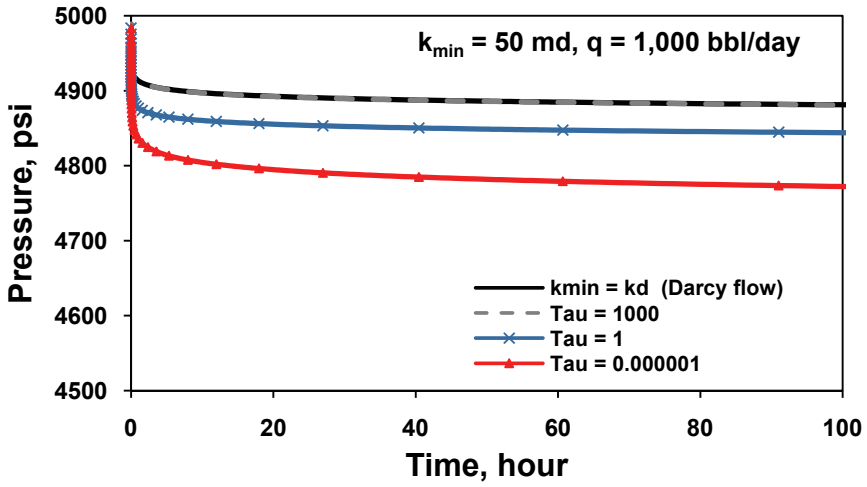

Figure 12 – Effect of non-Darcy flow characteristic length, τ, and low production rate on the pressure transient responses of drawdown test example using Barree and Conway model

Pressure Transient Analysis

In an effort to make the permeability estimate in presence of the non-Darcy flow effects, synthetic pressure transient responses generated using the numerical model incorporating the Barree and Conway model has been analyzed using the standard straight-line techniques. Synthetic pressure transient responses has been generated for two cases, (1) pressure drawdown test and (2) pressure drawdown test followed by pressure buildup test, to interpret non-Darcy flow effects on both pressure transient tests. Effects of skin (in case of formation damage) and wellbore storage on pressure transient responses has been analyzed considering effects of non-Darcy flow using the Barree and Conway model.

Pressure Drawdown Test Example

In this example, the porous-medium formation is assumed homogenous, radial, infinite acting and composed of a single layer of 100 ft thick. Simulation input data used for generating synthetic pressure transient responses is listed in Table 4. In numerical simulation, the porous-medium reservoir system is represented by a radially-symmetrical, cylindrical reservoir (RxZ, 10,000x100 ft) is discretized into a one-dimensional (R), the r-distance of 10,000 ft is subdivided into 2,010 volume elements in logarithmic scale with a Δr size that increases logarithmically away from the wellbore (r_w = 0.3 ft). The formation is initially at a constant pressure of 5,000 psi and is subjected to a constant production rate of 5,000 bbl/day at the producing well, starting at time of zero. The near wellbore effects including formation damage (skin effects) and/or wellbore storage has not been considered in this example to avoid interference with presence of non-Darcy flow effects. The Darcy's permeability is one of the input parameters used in the numerical model (k_d = 100 md). The Darcy's permeability can be estimated from the slope of the straight line (m) of a semi-log plot of wellbore pressure versus time as follow:

$$k_d = \frac{162.6 q \beta \mu}{m h} \tag{39}$$

Figure 13 shows the semi-log plot used for analysis of non-Darcy pressure transient responses. For the Darcy's flow case where the minimum permeability is set equal to the Darcy's permeability of 100 md, the estimated slope of the straight line is 81.8 psi/cycle and the estimated k_d is 99.5 md. This indicates that when k_{min} is equal to k_d in the Barree and Conway model, non-Darcy flow behavior is not present, we are simply analyzing Darcy's flow. The slope of the non-Darcy flow straight line is 90.5 psi/cycle and the re-estimated k_d is 89 md. This indicates that the non-Darcy flow behavior affects the estimation of the Darcy's permeability using the standard semi-log straight line analysis. The Barree and Conway model define and apparent permeability that account for both Darcy's and non-Darcy's flow combined in the following relationship:

$$k_{app} = k_{\min} + \frac{(k_d - k_{\min})}{(1 + \frac{\rho v}{\mu \tau})} \tag{40}$$

The fluid velocity in Eq. 40 is calculated from the production rate using the cross-sectional area to flow. The estimated k_{app} using Eq. 40, after unit conversions, is 54.5 md and is not equal to the value of the permeability estimated from the semi-log straight line analysis (89 md). This indicates that the estimated permeability from semi-log straight line is higher than the apparent permeability as predicted by Barree and Conway model (Eq. 40). In simulating pressure drawdown tests with the non-Darcy flow effects according to the Barree and Conway model and assuming no skin and wellbore storage effects the permeability estimated using the standard straight-line analysis is an apparent permeability and not the Darcy's constant permeability. The estimated permeability, in this example (89 md), ranges from the minimum permeability (k_{min} = 25 md) and to less than the Darcy's permeability (k_d = 100 md). Thus in pressure drawdown tests the standard straight-line analysis techniques underestimate the Darcy's permeability when non-Darcy flow behavior exists.

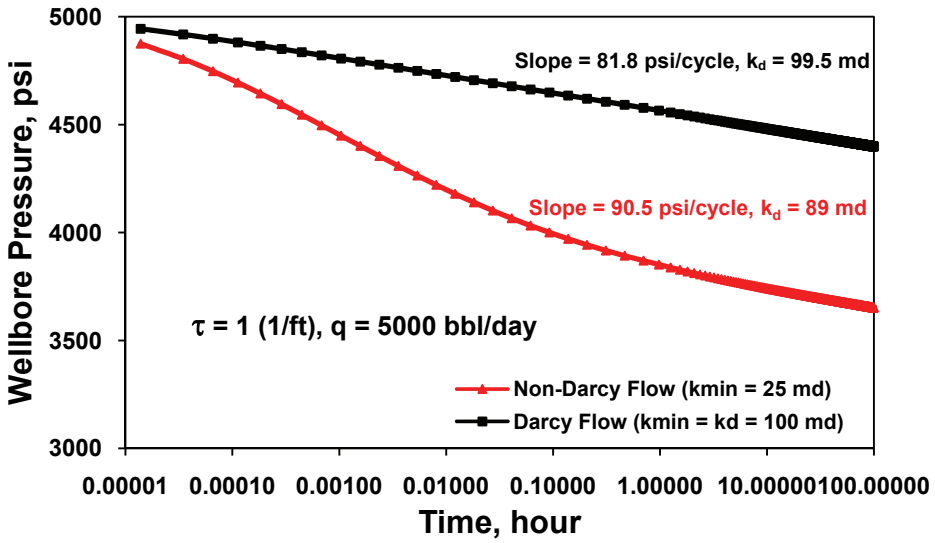

Figure 13 – Analysis of non-Darcy flow transient responses using Barree and Conway model of pressure drawdown test example

Pressure Drawdown followed by Pressure Buildup Test

In this example, the pressure drawdown test, discussed in previous example (input data used is listed in Table 4), is followed by a pressure buildup test. The pressure drawdown test lasts for 100 hours (production time) with a constant production rate of 5,000 bbl/day followed by shut-in of the well for 100 hours. Figure 14 presents the pressure-transient responses for the drawdown test followed by pressure buildup test generated, by the numerical simulator considering both Darcy's (k_{min} = 100 md) and non-Darcy's flow (k_{min} = 25 md) with a constant value for the characteristic length, τ, of 1 (1/ft). It is obvious that severe non-Darcy flow effects on the pressure-transient responses (during pressure drawdown) disappear completely during the pressure buildup test. This is simply because no production (or high velocity of produced fluid) during the pressure buildup period. Thus even with high non-Darcy flow effects (as simulated in this example) prior to pressure buildup test, the pressure transient responses afterward behaves like Darcy's flow responses. Analysis of permeability estimate using the standard straight-line techniques for the pressure buildup responses results in Darcy's constant permeability (k_d). Thus pressure buildup can be used to estimate k_d parameter of the Barree and Conway model with confidence even with strong non-Darcy flow effects during drawdown test prior to buildup test. As conclusion, if the pressure

drawdown test is followed by pressure buildup test then the estimation of the Darcy's permeability (k_d) parameter of the Barree and Conway model from the pressure buildup test is accurate even with severe non-Darcy flow behavior.

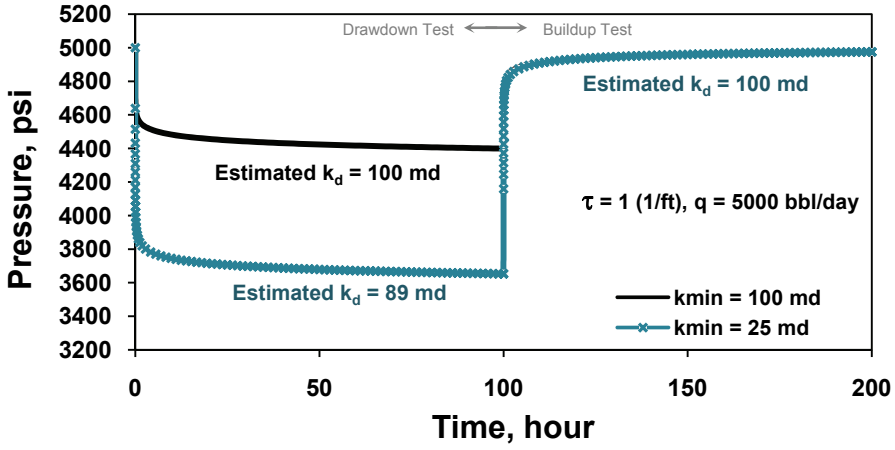

Figure 14 – Transient responses of a drawdown test followed by buildup test simulated using Barree and Conway model

Combined Effect of Skin, Wellbore Storage and Non-Darcy Flow

Figure 15 presents the pressure transient responses for the drawdown test discussed in the previous example including combined effects of skin and wellbore storage with the non-Darcy flow effects. The wellbore storage (C = 0.1 bbl/psi) with non-Darcy flow effects (k_{min} = 25 md, τ = 1 1/ft) only affects the early time responses and does not affect the permeability estimate. The skin (S = 1) causes a high pressure drop with the non-Darcy flow effects. The combined effect of both wellbore storage and skin is shown in Figure 15. The interpretation of all pressure transient responses shows the same results as obtained before, the non-Darcy flow behavior affects the estimate of constant Darcy's permeability using the standard straight-line techniques.

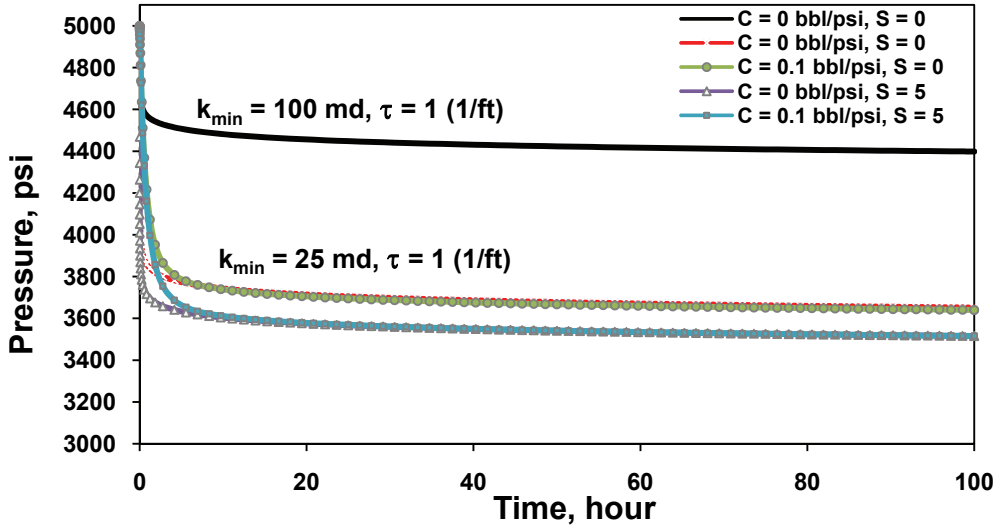

Figure 15 – Combined effects of wellbore storage and skin on pressure drawdown test simulated using Barree and Conway model

Estimation of Non-Darcy Flow Parameters

Since non-Darcy flow parameters of the Barree and Conway model (k_{min} and τ) may not be directly estimated from pressure-transient data, we developed a methodology to obtain these parameters indirectly. This methodology is based on matching actual pressure-transient data with transient responses generated by the numerical model by incorporating a non-linear optimization algorithm, based on non-linear Gauss-Levenberg algorithm. For a given producing well, constant Darcy's permeability (k_d) is estimated from analysis of actual pressure buildup test data, as discussed in previous examples, using standard straight-line analysis and then input to the numerical model with well and reservoir data. Then numerical model is run with non-linear optimization algorithm to match actual pressure-transient data and report non-Darcy flow parameters of the Barree and Conway model (k_{min} and τ) for the matched case. This matching process takes sometimes more iterations and requires an initial guess of two parameters and their range of values for non-linear optimization algorithm to work. This procedure is only valid for pressure drawdown test data where non-Darcy flow behavior exists (high production rate) and may not be applied to pressure buildup data since non-Darcy flow effects disappears completely after shut-in of the well.

Analysis of Field Pressure Drawdown and Buildup Tests

Actual pressure transient data (drawdown and buildup tests) from high production rate wells in Kuwait have been analyzed to understand non-Darcy flow effects using the numerical model of this study incorporating Barree and Conway model and non-linear optimization method. As an application example, we show here analysis results of actual pressure drawdown test followed by pressure buildup test (for high-rate oil producer well in Kuwait) to estimate non-Darcy flow parameters of the Barree and Conway model. Input data for well and reservoir used in numerical simulation are listed in Table 5. Figure 16 shows actual transient pressure data for the studied well for pressure drawdown test followed by pressure buildup test. Analysis of pressure buildup test data shows that k_d = 449.89 md, S_t = 11.29 and C = 0.829 bbl/psi using standard well testing techniques. Figure 17 shows semi-log plot of wellbore pressure versus time for actual pressure drawdown data and numerical model of this study (matched, optimized case). Figure 17 indicates that excellent results are obtained from optimized numerical simulation, as compared to actual well test data. The estimated non-Darcy flow parameters of Barree and Conway model for the matched case of pressure drawdown test are k_{min} = 126.46 md and τ = 0.552 (1/ft). These results and information can be used to model accurately non-Darcy flow to predict and improve well and reservoir performance.

Table 5 - Input data used for numerical simulation and transient analysis of non-Darcy flow using Barree and Conway model for pressure drawdown test followed by pressure buildup for a high-rate oil producing well in Kuwait

Parameter	Value	Unit
Porosity	ϕ = 0.26	
Viscosity	μ = 0.162	cp
Initial Pressure before Test	P_i = 3,288.62	psi
Production Rate	q = 6,195	stb/day
Oil Formation Volume Factor	B_o = 1.69	bbl/stb
Formation Thickness	h = 159	ft
Reservoir Drainage Radius	r_e = 10,000	ft
Total Compressibility	$c_t = 2.378 \times 10^{-5}$	psi^{-1}
Wellbore Radius	r_w = 0.31	ft
Duration of Drawdown Test	24	hours
Duration of Buildup Test	68	hours

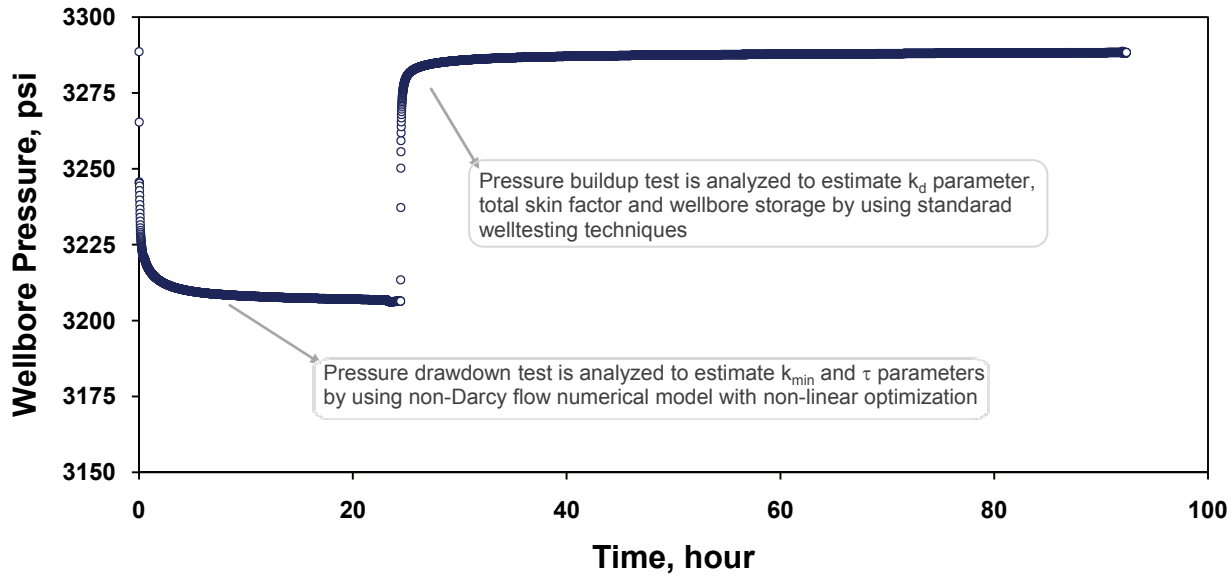

Figure 16 – Actual pressure-transient data for pressure drawdown test followed by buildup test for high production rate well in Kuwait

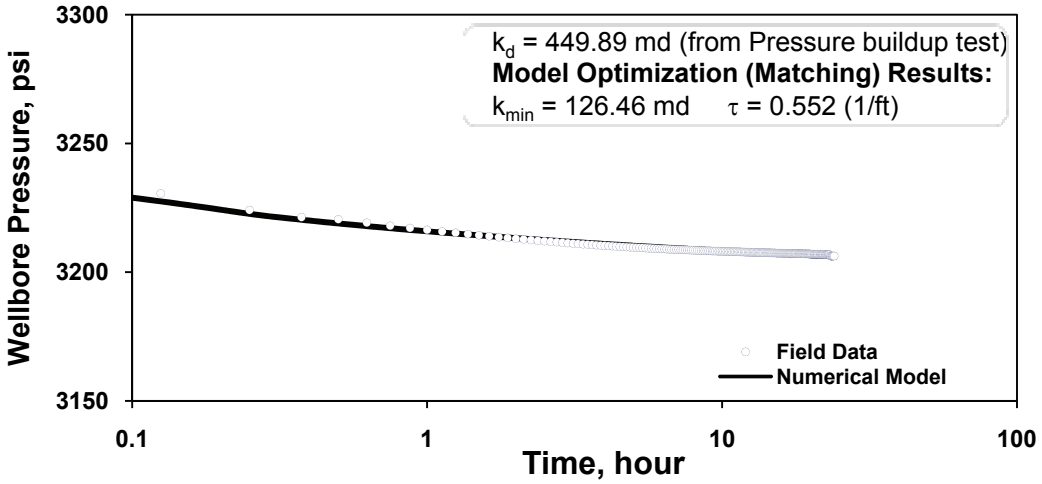

Figure 17 – Estimation of non-Darcy flow parameters of Barree and Conway model from actual pressure drawdown test data for high production rate well in Kuwait using non-linear optimized numerical model

Conclusions

In this paper, we have presented the usage of the Barree and Conway model in pressure-transient analysis of non-Darcy flow in porous-medium and fractured reservoirs. The non-Darcy fluid flow according to the Barree and Conway model is incorporated into a three-dimensional reservoir simulator. The developed numerical model is capable of simulating all near wellbore effects, such as the wellbore storage and skin effects with the non-Darcy flow behavior. An analytical solution for steady-state non-Darcy radial flow has been derived according to the Barree and Conway model and is used to verify the numerical model. The numerical model has been used to model and interpret the radial flow pressure-transient responses for pressure buildup and drawdown well tests in porous-medium and fractured reservoirs. The following conclusions are obtained from the work presented in this paper:

1. The Barree and Conway model can be applied to analyze and interpret transient behavior of non-Darcy flow in both porous-medium and fractured reservoirs.
2. In simulating pressure drawdown tests with the non-Darcy flow effects according to Barree and Conway model without skin and wellbore storage effects, the permeability obtained using the standard straight-line analysis is an apparent permeability and not the Darcy's constant permeability. The estimated permeability ranges from the minimum permeability and to less than the Darcy's permeability. In pressure drawdown tests the standard straight-line analysis techniques underestimate the Darcy's permeability when non-Darcy flow behavior exists.
3. A pressure buildup test, following non-Darcy flow drawdown tests, may be good for determining Darcy's permeability values using the standard straight-line analysis without significant non-Darcy flow.
4. Type curves generated by the optimized numerical model are provided to demonstrate a methodology for modeling single phase transient non-Darcy flow behavior in porous-medium and fractured rocks.
5. The Barree and Conway non-Darcy flow model parameters may not be directly estimated from the pressure-transient well tests using conventional analysis approaches. However, they can be estimated by a matching process based on non-linear optimization algorithm incorporated into the developed numerical model in this study.
6. The developed numerical model from this study can be used to interpret and match actual pressure drawdown and buildup well tests from high production rate wells and to estimate non-Darcy flow parameters according to the Barree and Conway model. These results and information can be used to accurately model non-Darcy flow and to predict and improve well and reservoir performance.

Acknowledgements

The authors would like to thank the management of Kuwait Oil Company (KOC) for the help in providing pressure transient data used in this study. Parts of this work will appear in the PhD dissertation of Ajab Al-Otaibi. The financial support for Mr. Ajab Al-Otaibi graduate studies at the Colorado School of Mines has been provided by Kuwait Government.

Nomenclature

P	=	pressure, psi
t	=	time, hour
$\partial P/\partial L$	=	pressure (head or potential) gradient, psi/ft
μ	=	fluid viscosity, cp
k	=	formation permeability, Darcy or md
v	=	superficial velocity, ft/s
β	=	non-Darcy flow coefficient, 1/ft

ρ	=	fluid density, lbm/ft^3
γ	=	non-Darcy flow coefficient in Forchheimer's cubic Eq., 1/ft
ϕ	=	formation porosity, fraction
S	=	skin factor, dimensionless
D	=	non-Darcy flow coefficient, day/stb or day/Mscf
d	=	distance, ft
h	=	formation net-pay thickness, ft
k	=	permeability, md
R_e	=	Reynolds number, dimensionless
R_p	=	pseudo-Reynolds number, 1/ft
τ	=	characteristic length, 1/ft
q	=	volumetric flow rate, bbl/day
$\dot{m}$	=	mass flow rate, lbm/day
r	=	distance in radial direction, ft
Φ	=	flow potential, psi
g	=	gravitational acceleration, ft/s^2
D	=	depth, ft
B	=	formation volume factor, bbl/stb
V	=	volume, bbl
A	=	area of interface, ft^2
F	=	mass flow term, lbm/day
Q	=	mass sink/source term
λ	=	mobility of flowing fluid phase, md/cp
N	=	total number of nodes, elements or grid blocks
R	=	residual, dimensionless
x	=	primary variable
Δt	=	time step size, hour
C_t	=	total compressibility, psi^{-1}
C	=	wellbore storage coefficient, bbl/psi
V_{wb}	=	wellbore volume, bbl
c_{wb}	=	compressibility of wellbore fluid, psi^{-1}
m	=	slope of semi-log plot straight-line, psi/cycle

Superscript

E, F	=	exponents
n	=	current time level
$n+1$	=	next time level to be solved

Subscript

t	=	total
i	=	initial
M	=	mechanical
s	=	skin zone
app	=	apparent
min	=	minimum
p	=	pseudo
d	=	Darcy
D	=	Dimensionless
mr	=	minimum relative
β	=	fluid phase (could be oil or gas)
x, y, z	=	x-, y-, z- directions, respectively
r, θ	=	r-, θ- directions, respectively
i, j	=	arbitrary element or node
$ij+1/2$	=	proper averaging of properties at the interface between the two elements i, j
p	=	iteration level
w	=	well
wb	=	wellbore
e	=	outer boundary

References

Muskat, M. (1946). The Flow of Homogeneous Fluids through Porous Media, J. W. Edwards, Inc., Ann Arbor, Michigan.

Forchheimer, P. (1901). Wasserbewegung durch Bode, ZVDI 45.

Ramey, H.J. Jr. (1965). Non-Darcy Flow and Wellbore Storage Effects in Pressure Build-Up and Drawdown of Gas Wells, JPT (Feb.) 223, Trans., AIME, 234.

Firoozabadi, A. and Katz, D.L. (1979). An Analysis of High-Velocity Gas Flow through Porous media, JPT (Feb.), 211-216.

Odeh, A.S., Moreland, E.E. and Schueler, S. (1975). Characterization of a Gas Well From One Flow-Test Sequence, JPT (Dec.), 1500-1504.

Scheidegger, A.E. (1974). The Physicals of Flow through Porous Media, University of Toronto Press, Toronto.

Tek, M.R., Coats, K.H. and Katz, D.L. (1962). The effects of turbulence on flow of natural gas through porous reservoirs, JPT, Trans., AIME, Vol. 222, 799-806.

Katz, D.L. and Lee, R.L. (1990). Natural Gas Engineering, Production and Storage, Chemical Engineering Series, McGraw-Hill Book Co. Inc., New York.

Smith, R.V. (1961). Unsteady-State Gas Flow into Gas Wells, JPT (Nov.) 1151.

Swift, G.W. and Kiel, O.G. (1962). The Prediction of Gas-Well Performance Including the Effect of Non-Darcy Flow, JPT (Jul.) 791; Trans., AIME, 225.

Holditch, S.A. and Morse, R.A. (1976). The Effects of Non-Darcy Flow on the Behavior of Hydraulically Fractured Gas Wells, JPT (Oct.) 1169.

Guppy, K.H. et al. (1982). Non-Darcy Flow in Wells With Finite-Conductivity Fractures, SPEJ (Oct.) 681.

Gidley, J.L. (1991). A Method for Correcting Dimensionless Fracture Conductivity for Non-Darcy Flow Effects, SPEPE (Nov.) 391.

Settari, A., Stark, A.J. and Jones, J.R. (2000). Analysis of Hydraulic Fracturing of High Permeability Gas Wells to Reduce Non-Darcy Skin Effects, J. Cdn. Pet. Tech. (May) 39, 56.

Cullender, M.H. (1955). The Isochronal Performance Method of Determining the Flow Characteristics of Gas Wells, JPT (Sep.) 137-42; Trans., AIME 204.

Jones, L.G., Blount, E.M. and Glaze, O.H. (1975). Use of Short Term Multiple Rate Flow Tests to Predict Performance of Wells Having Turbulence, SPE 6133, SPE Annual Technical Conference and Exhibition, New Orleans, 3-6 October.

Brar, G.S. and Aziz, K. (1978). The Analysis of Modified Isochronal Tests to Predict the Stabilized Deliverability of Gas Wells without Using Stabilized Flow Data, JPT (Feb.) 297-304.

Kelkar, M.G. (2000). Estimation of Turbulence Coefficient Based on Field Observation, SPE Reservoir Evaluation and Engineering (April) 160-164.

Fetkovich, M.J. (1973). The Isochronal Testing of Oil Wells, SPE 4529, SPE Annual Meeting, Las Vegas, Nevada, 30 Sep.–3 October.

Himmatramka, A.K. (1981). Analysis of Productivity Reduction Due to Non-Darcy Flow and True Skin in Gravel-Packed Wells, SPE 10084, SPE Annual Technical Conference and Exhibition, San Antonio, Texas, 5–7 October.

Blacker, L.K. (1982). An Analysis of Rate-Sensitive Skin in Oil Wells, SPE 11187, SPE Annual Technical Conference and Exhibition, New Orleans, 26–29 September.

Carman, P.C. (1937). Fluid Flow Through Granular Beds. Transactions Institution of Chemical Engineers 15 (150).

Fand, R.M., Kim, B.Y.K, Lam, A.C.C. and Phan, R.T. (1987). Resistance to the Flow of Fluids Through Simple and Complex Porous Media Whose Matrices Are Composed of Randomly Packed Spheres, Transactions of the ASME 109 (268).

Montillet, A. (2004). Flow Through a Finite Packed Bed of Spheres: A Note on the Limit of Applicability of the Forchheimer Type Equation. Journal of Fluids Engineering 126 (139).

Barree, R.D. and Conway, M.W. (2004). Beyond Beta Factors: A Complete Model for Darcy, Forchheimer and Trans-Forchheimer Flow in Porous Media. SPE 89325, SPE Annual Technical Conference and Exhibition, Houston, Texas 26-29 September.

Barree, R.D. and Conway, M.W. (2005). Reply to Discussion of; Beyond Beta Factors, A Complete Model for Darcy, Forchheimer, and Trans-Forchheimer Flow in Porous Media. JPT 57 (8): 73-74.

Lai, B., Miskimins, J.L. and Wu, Y.S. (2009). Non-Darcy Porous Media Flow According to the Barree and Conway Model: Laboratory and Numerical Modeling Studies. SPE 122611, SPE Rocky Mountain Petroleum Technology Conference, Denver, Colorado 14-16 April.

Narasimhan, T. N. and P. A. Witherspoon (1976). An Integrated Finite Difference Method for Analyzing Fluid Flow in Porous Media, Water Resources Research, 12 (1), pp. 57–64.

Pruess, K., Oldenburg, C. and Moridis, G. (1999). TOUGH2 User's Guide, Version 2.0, Report LBNL-43134, Berkeley, California, Lawrence Berkeley National Laboratory.

Wu, Y.S. (2002). Numerical Simulation of Single-Phase and Multiphase Non-Darcy Flow in Porous and Fractured Reservoirs. Transport in Porous Media 49 (2): 209-240.

Clift, S.S., Aevedo E.F., Forsyth P.A., and Knightly, J.R. (1996). WATSIT-1 and WATSIT-B, Waterloo Sparse, Iterative Matrix Solvers, User's Guide with Developer Notes for Version 2.0.0, Department of Computer Science, University of Waterloo, Waterloo, Ontario, Canada, August 1996.

Forsyth, P.A., Wu, Y.S. and Pruess, K. (1995). Robust Numerical Methods for Saturated-Unsaturated Flow with Dry Initial Conditions in Heterogeneous Media, Advances in Water Resources, Vol. 18, pp. 25-38.

Wu, Y.S. (2000). A virtual node method for handling wellbore boundary conditions in modeling multiphase flow in porous and fractured media. Water Resources Research 36 (3): 807-814.

Wu, Y.S., Forsyth, P.A. and Jiang, H. (1996). A consistent approach for applying numerical boundary conditions for subsurface flow, Journal of Contaminant Hydrology 23: 157-185.

Hawkins, M.F. Jr. (1956). A note on the Skin Effect, Trans. AIME, 207: 356-357.

Barenblatt, G.I., Zheltov, I.P. and Kochina, I.N. (1960). Basic Concepts in the Theory of Seepage of Homogeneous Liquids in Fissured Rocks, PMM, Sov. Appl. Math. Mech., 24(5), 852-864.

Warren, J.E. and Root, P.J. (1963). The Behavior of Naturally Fractured Reservoirs, Soc. Pet. Eng. J., Trans., AIME, 228, pp. 245-255, September 1963.

Kazemi, H. (1969). Pressure Transient Analysis of Naturally Fractured Reservoirs with Uniform Fracture Distribution. SPEJ, 451-62. Trans., AIME, 246.
Pruess, K. and Narasimhan, T.N. (1985). A practical method for modeling fluid and heat flow in fractured porous media, Soc. Pet. Eng. J., 25, pp.14-26.
Wu, Y.S. and Pruess, K. (1988). A multiple-porosity method for simulation of naturally fractured petroleum reservoirs, SPE Reservoir Engineering, 3, pp. 327-336.
Pruess, K. (1991). TOUGH2 - A General-Purpose Numerical simulator for multiphase fluid and heat flow, Report LBL-29400, Lawrence Berkeley National Laboratory, Berkeley, California.
Pruess, K. (1983). GMINC - A mesh generator for flow simulations in fractured reservoirs, Report LBL-15227, Lawrence Berkeley National Laboratory, Berkeley, California.
Wu, Y.S. (1998). MSFLOW: Multiphase Subsurface Flow Model of Oil, Gas and Water in Porous and Fractured Media with Water Shut-off Capability, Documentation and User's Guide, Walnut Creek, California.

Appendix A. Derivations of Steady-State Flow Solution in a 1-D Radial Reservoir for Incompressible, Slightly Compressible and Compressible Fluids According to the Barree and Conway Flow Model

The relationship between pressure gradient and fluid velocity according to the Barree and Conway model for single-phase fluid flow in 1-D radial reservoir is given by

$$\frac{\partial P}{\partial r} = \frac{\mu \mathrm{v}}{k_d \left(k_{mr} + \frac{(1-k_{mr})}{(1+\rho \mathrm{v}/\mu\tau)} \right)} \tag{A1}$$

Recasting Eq. A1

$$k_d k_{mr} \rho \mathrm{v} \frac{\partial P}{\partial r} + k_d \mu\tau \frac{\partial P}{\partial r} = \mu^2 \tau \mathrm{v} + \mu\rho \mathrm{v}^2 \tag{A2}$$

Rearranging Eq. A2

$$\mu\rho \mathrm{v}^2 + (\mu^2\tau - k_d k_{mr} \rho \frac{\partial P}{\partial r})\mathrm{v} - k_d \mu\tau \frac{\partial P}{\partial r} = 0 \tag{A3}$$

Solving Eq. A3 for fluid velocity and considering only the positive root (valid) solution

$$\mathrm{v} = \frac{-(\mu^2\tau - k_d k_{mr} \rho \frac{\partial P}{\partial r}) + \sqrt{(\mu^2\tau - k_d k_{mr} \rho \frac{\partial P}{\partial r})^2 + 4\mu^2 \rho k_d \tau \frac{\partial P}{\partial r}}}{2\mu\rho} \tag{A4}$$

The continuity equation for steady-state radial flow in porous media is given by

$$\frac{\partial}{\partial x}(\rho \mathrm{v}) = 0 \tag{A5}$$

Integrating Eq. A5 leads to

$$\rho \mathrm{v} = C \tag{A6}$$

According to flow velocity and mass flow rate definition, we have

$$\rho \mathrm{v} = \rho \frac{Q}{A} = \frac{\dot{m}}{A} \tag{A7}$$

Substituting Eq. A4 into Eq. A7

$$\rho\frac{-(\mu^2\tau - k_d k_{mr}\rho\frac{\partial P}{\partial r}) + \sqrt{(\mu^2\tau - k_d k_{mr}\rho\frac{\partial P}{\partial r})^2 + 4\mu^2\rho k_d\tau\frac{\partial P}{\partial r}}}{2\mu\rho} = \frac{\dot{m}}{A} \tag{A8}$$

For a 1D radial reservoir the cross-sectional area is given by

$$A = 2\pi rh \tag{A9}$$

Substituting Eq. A9 into Eq. A8

$$\rho\frac{-(\mu^2\tau - k_d k_{mr}\rho\frac{\partial P}{\partial r}) + \sqrt{(\mu^2\tau - k_d k_{mr}\rho\frac{\partial P}{\partial r})^2 + 4\mu^2\rho k_d\tau\frac{\partial P}{\partial r}}}{2\mu\rho} = \frac{\dot{m}}{2\pi rh} \tag{A10}$$

Rearranging Eq. A10

$$-(\mu^2\tau - k_d k_{mr}\rho\frac{\partial P}{\partial r}) + \sqrt{(\mu^2\tau - k_d k_{mr}\rho\frac{\partial P}{\partial r})^2 + 4\mu^2\rho k_d\tau\frac{\partial P}{\partial r}} = \mu\frac{\dot{m}}{\pi rh} \tag{A11}$$

Recasting Eq. A11

$$\sqrt{(\mu^2\tau - k_d k_{mr}\rho\frac{\partial P}{\partial r})^2 + 4\mu^2\rho k_d\tau\frac{\partial P}{\partial r}} = \mu\frac{\dot{m}}{\pi rh} + (\mu^2\tau - k_d k_{mr}\rho\frac{\partial P}{\partial r}) \tag{A12}$$

Eliminating the square root in Eq. A12

$$(\mu^2\tau - k_d k_{mr}\rho\frac{\partial P}{\partial r})^2 + 4\mu^2\rho k_d\tau\frac{\partial P}{\partial r} = (\mu\frac{\dot{m}}{\pi rh} + (\mu^2\tau - k_d k_{mr}\rho\frac{\partial P}{\partial r}))^2 \tag{A13}$$

Recasting Eq. A13

$$(\mu^2\tau - k_d k_{mr}\rho\frac{\partial P}{\partial r})^2 + 4\mu^2\rho k_d\tau\frac{\partial P}{\partial r} = (\mu\frac{\dot{m}}{\pi rh})^2 + (\mu^2\tau - k_d k_{mr}\rho\frac{\partial P}{\partial r})^2 + 2*\mu\frac{\dot{m}}{\pi rh}*(\mu^2\tau - k_d k_{mr}\rho\frac{\partial P}{\partial r}) \tag{A14}$$

Simplifying Eq. A14

$$\mu\rho k_d\tau\frac{\partial P}{\partial r} = \mu(\frac{\dot{m}}{2\pi rh})^2 + \frac{\dot{m}}{2\pi rh}\mu^2\tau - \frac{\dot{m}}{2\pi rh}k_d k_{mr}\rho\frac{\partial P}{\partial r} \tag{A15}$$

Rearranging Eq. A15

$$2\pi rh\,\mu\rho k_d\tau\frac{\partial P}{\partial r} = \mu\frac{\dot{m}^2}{2\pi rh} + \dot{m}\mu^2\tau - \dot{m}k_d k_{mr}\rho\frac{\partial P}{\partial r} \tag{A16}$$

$$\left(2\pi rh\,\mu\tau + \dot{m}k_{mr}\right)k_d\rho\frac{\partial P}{\partial r} = \mu\frac{\dot{m}^2}{2\pi rh} + \dot{m}\mu^2\tau \tag{A17}$$

Rearranging and integrating Eq. A17

$$k_d\int\rho dP = \int\frac{\left(\mu\frac{\dot{m}^2}{2\pi rh} + \dot{m}\mu^2\tau\right)}{\left(2\pi rh\,\mu\tau + \dot{m}k_{mr}\right)}dr \tag{A18}$$

To simplify the solution let us assume the following:

$$c_1 = \frac{\mu \dot{m}^2}{2\pi h} \tag{A19}$$

$$c_2 = \dot{m}\,\mu^2 \tau \tag{A20}$$

$$c_3 = 2\pi h\,\mu\tau \tag{A21}$$

$$c_4 = \dot{m} k_{mr} \tag{A22}$$

Rewriting Eq. A18 using Eqs. A19-A22

$$k_d \int \rho dP = \int \frac{\left(\frac{c_1}{r} + c_2\right)}{c_3 r + c_4} dr \tag{A23}$$

Assuming incompressible single-phase ($\rho = \rho_i$) flow and solving Eq. A23

$$k_d \rho_i P = \frac{c_1 \ln(r)}{c_4} + \frac{\left(-c_1 c_3 + c_2 c_4\right)\ln\left(c_4 + c_3 r\right)}{c_3 c_4} + C \tag{A24}$$

Applying the boundary limits on Eq. A23

$$k_d \int_{P_i}^{P} \rho dP = \int_{r_e}^{r} \frac{\left(\frac{c_1}{r} + c_2\right)}{c_3 r + c_4} dr \tag{A25}$$

Solving Eq. A25 using the solution in Eq. A24 and considering the boundary conditions

$$k_d \rho_i \left(P - P_i\right) = \left[\frac{c_1 \ln(r)}{c_4} + \frac{\left(-c_1 c_3 + c_2 c_4\right)\ln\left(c_4 + c_3 r\right)}{c_3 c_4}\right] - \left[\frac{c_1 \ln r_e}{c_4} + \frac{\left(-c_1 c_3 + c_2 c_4\right)\ln\left(c_4 + c_3 r_e\right)}{c_3 c_4}\right] \tag{A26}$$

Simplifying Eq. A26

$$k_d \rho_i \left(P - P_i\right) = \frac{c_1}{c_4}\ln\left(\frac{r}{r_e}\right) + \frac{\left(-c_1 c_3 + c_2 c_4\right)}{c_3 c_4}\ln\left(\frac{c_4 + c_3 r}{c_4 + c_3 r_e}\right) \tag{A27}$$

Rearranging Eq. A27

$$P = P_i - \frac{1}{k_d \rho_i}\left[\frac{c_1}{c_4}\ln\left(\frac{r_e}{r}\right) - \frac{\left(-c_1 c_3 + c_2 c_4\right)}{c_3 c_4}\ln\left(\frac{c_4 + c_3 r_e}{c_4 + c_3 r}\right)\right] \tag{A28}$$

Substituting Eqs. A19-A22 in Eq. A28

$$P = P_i - \frac{1}{k_d \rho_i}\left[\frac{\frac{\mu \dot{m}^2}{2\pi h}}{\dot{m} k_{mr}}\ln\left(\frac{r_e}{r}\right) - \frac{\left(-\frac{\mu \dot{m}^2}{2\pi h}\left(2\pi h\,\mu\tau\right) + \dot{m}\,\mu^2 \tau \dot{m} k_{mr}\right)}{\left(2\pi h\,\mu\tau\right)\dot{m} k_{mr}}\ln\left(\frac{\dot{m} k_{mr} + \left(2\pi h\,\mu\tau\right) r_e}{\dot{m} k_{mr} + \left(2\pi h\,\mu\tau\right) r}\right)\right] \tag{A29}$$

Simplifying Eq. A29

$$P = P_i - \frac{1}{k_d \rho_i}\left[\frac{\mu \dot{m}}{2\pi h k_{mr}}\left\{\ln\left(\frac{r_e}{r}\right) - \left(k_{mr} - 1\right)\ln\left(\frac{\dot{m} k_{mr} + \left(2\pi h \mu\tau\right) r_e}{\dot{m} k_{mr} + \left(2\pi h \mu\tau\right) r}\right)\right\}\right] \tag{A30}$$

Eq. A30 is the steady-state analytical solution for radial flow of incompressible fluid using the Barree and Conway model.

For single phase slightly compressible liquid flow

$$\rho = \rho_i \exp\left(c\left(P - P_i\right)\right) \tag{A31}$$

In porous media flow, Eq. A31 is usually simplified as

$$\rho = \rho_i \left(1 + c\left(P - P_i\right)\right) \tag{A32}$$

Substituting Eq. A32 in Eq. A23

$$k_d \int \rho_i \left(1 + c\left(P - P_i\right)\right) dP = \int \frac{\left(\frac{c_1}{r} + c_2\right)}{c_3 r + c_4} dr \tag{A33}$$

Solving Eq. A33 assuming the compressibility is constant (usual case for liquid flow)

$$k_d \rho_i \left[\left(1 - cP_i\right)P + \frac{c}{2}P^2\right] = \frac{c_1 \ln r}{c_4} + \frac{\left(-c_1 c_3 + c_2 c_4\right)\ln\left(c_4 + c_3 r\right)}{c_3 c_4} + C \tag{A34}$$

Applying the boundary limits on Eq. A40

$$k_d \int_{P_i}^{P} \rho_i \left(1 + c\left(P - P_i\right)\right) dP = \int_{r_e}^{r} \frac{\left(\frac{c_1}{r} + c_2\right)}{c_3 r + c_4} dr \tag{A35}$$

Solving Eq. A35 using the solution in Eq. A24 and considering the boundary conditions and further rearranging and simplifying

$$\frac{c}{2}P^2 + \left(1 - cP_i\right)P - \left(1 - cP_i\right)P_i - \frac{c}{2}P_i^2 = \frac{1}{k_d \rho_i}\left[\frac{c_1}{c_4}\ln\left(\frac{r}{r_e}\right) + \frac{\left(-c_1 c_3 + c_2 c_4\right)}{c_3 c_4}\ln\left(\frac{c_4 + c_3 r}{c_4 + c_3 r_e}\right)\right] \tag{A36}$$

Substituting Eqs. A19-A22 in Eq. A36 and simplifying

$$\frac{c}{2}P^2 + \left(1 - cP_i\right)P - \left(1 - cP_i\right)P_i - \frac{c}{2}P_i^2 = \frac{1}{k_d \rho_i}\left[\frac{\mu \dot{m}}{2\pi h k_{mr}}\left\{\ln\left(\frac{r_e}{r}\right) - \left(k_{mr} - 1\right)\ln\left(\frac{\dot{m} k_{mr} + \left(2\pi h \mu\tau\right) r_e}{\dot{m} k_{mr} + \left(2\pi h \mu\tau\right) r}\right)\right\}\right] \tag{A37}$$

Recasting Eq. A37

$$\frac{c}{2}P^2 + \left(1 - cP_i\right)P - \left\{\left(1 - cP_i\right)P_i - \frac{c}{2}P_i^2 - \frac{1}{k_d \rho_i}\left[\frac{\mu \dot{m}}{2\pi h k_{mr}}\left\{\ln\left(\frac{r_e}{r}\right) - \left(k_{mr} - 1\right)\ln\left(\frac{\dot{m} k_{mr} + \left(2\pi h \mu\tau\right) r_e}{\dot{m} k_{mr} + \left(2\pi h \mu\tau\right) r}\right)\right\}\right]\right\} = 0 \tag{A38}$$

Eq. A38 can be solved in term of pressure P as follow

$$P = \frac{-(1-cP_i) \pm \sqrt{(1-cP_i)^2 + 2c\left\{\left(1-\frac{c}{2}P_i\right)P_i + \frac{1}{k_d \rho_i}\left[\frac{\mu \dot{m}}{2\pi h k_{mr}}\left\{\ln\left(\frac{r_e}{r}\right) - (k_{mr}-1)\ln\left(\frac{\dot{m}k_{mr} + (2\pi h \mu\tau) r_e}{\dot{m}k_{mr} + (2\pi h \mu\tau) r}\right)\right\}\right]\right\}}}{c} \quad \text{(A39)}$$

The pressure P at any radial distance r is the positive root of Eq. A39. Equation A39 is the steady-state analytical solution for radial flow of slightly compressible liquids using the Barree and Conway model.

For single phase gas flow (compressible fluid), the density is described by the real gas law

$$\rho = \frac{PM}{zRT} \quad \text{(A40)}$$

Substituting Eq. A40 in Eq. A23 and applying the boundary limits

$$k_d \int_{P_i}^{P} \frac{PM}{zRT} dP = \int_{r_e}^{r} \frac{\left(\frac{c_1}{r} + c_2\right)}{c_3 r + c_4} d \quad \text{(A41)}$$

Substituting Eqs. A19-A22 in Eq. A41 and solving

$$\frac{M}{RT} \int_{P_i}^{P} \frac{P}{z} dP = \frac{\mu \dot{m}}{2\pi h k_{mr} k_d}\left\{\ln\left(\frac{r_e}{r}\right) - (k_{mr}-1)\ln\left(\frac{\dot{m}k_{mr} + (2\pi h \mu\tau) r_e}{\dot{m}k_{mr} + (2\pi h \mu\tau) r}\right)\right\} \quad \text{(A42)}$$

Eq. A42 is the steady-state analytical solution for radial flow of compressible gas using the Barree and Conway model.